Taylor & Francis
Taylor & Francis Group

Journal of Biomaterials Science, Polymer Edition

ISSN: 0920-5063 (Print) 1568-5624 (Online) Journal homepage: https://www.tandfonline.com/loi/tbsp20

Measuring fiber alignment in electrospun scaffolds: a user's guide to the 2D fast Fourier transform approach

Chantal E. Ayres, B. Shekhar Jha, Hannah Meredith, James R. Bowman, Gary L. Bowlin, Scott C. Henderson & David G. Simpson

To cite this article: Chantal E. Ayres, B. Shekhar Jha, Hannah Meredith, James R. Bowman, Gary L. Bowlin, Scott C. Henderson & David G. Simpson (2008) Measuring fiber alignment in electrospun scaffolds: a user's guide to the 2D fast Fourier transform approach, Journal of Biomaterials Science, Polymer Edition, 19:5, 603-621, DOI: 10.1163/156856208784089643

To link to this article: https://doi.org/10.1163/156856208784089643

Published online: 02 Apr 2012.

Submit your article to this journal

Article views: 1622

View related articles

Citing articles: 45 View citing articles

Full Terms & Conditions of access and use can be found at
https://www.tandfonline.com/action/journalInformation?journalCode=tbsp20

EMBZIM EX1010

J. Biomater. Sci. Polymer Edn, Vol. 19, No. 5, pp. 603–621 (2008)
© Koninklijke Brill NV, Leiden, 2008.
Also available online - www.brill.nl/jbs

Review

Measuring fiber alignment in electrospun scaffolds: a user's guide to the 2D fast Fourier transform approach

CHANTAL E. AYRES [1], B. SHEKHAR JHA [2], HANNAH MEREDITH [2], JAMES R. BOWMAN [2], GARY L. BOWLIN [1], SCOTT C. HENDERSON [2] and DAVID G. SIMPSON [2,*]

[1] *Department of Biomedical Engineering, Virginia Commonwealth University, Richmond, VA 23116, USA*
[2] *Department of Anatomy and Neurobiology, Virginia Commonwealth University, Richmond, VA 23116, USA*

Received 9 October 2006; accepted 18 July 2007

Abstract—In this study we describe how to use a two-dimensional fast Fourier transform (2D FFT) approach to measure fiber alignment in electrospun materials. This image processing function can be coupled with a variety of imaging modalities to assign an objective numerical value to scaffold anisotropy. A data image of an electrospun scaffold is composed of pixels that depict the spatial organization of the constituent fibers. The 2D FFT function converts this spatial information into a mathematically defined frequency domain that maps the rate at which pixel intensities change across the original data image. This output image also contains quantitative information concerning the orientation of objects in a data image. We discuss the theory and practice of using the frequency plot of the 2D FFT function to measure relative scaffold anisotropy and identify the principal axis of fiber orientation. We note that specific degrees of scaffold anisotropy may represent a critical design feature in the fabrication of tissues that will be subjected to well-defined uniaxial mechanical loads. This structural property may also represent a source of guidance cues that can be exploited to regulate cell phenotype.

Key words: 2D fast Fourier transform; fiber alignment; electrospinning; scaffold; data imaging.

INTRODUCTION

Electrospinning technology shows great potential as a gateway to the development of physiologically relevant tissue-engineering scaffolds [1]. This non-mechanical process has been used to fabricate natural protein polymers [2–4], biocompatible synthetic polymers [5, 6] and blends of natural and synthetic polymers [7, 8]

*To whom correspondence should be addressed. E-mail: dgsimpso@vcu.edu

into tissue-engineering scaffolds composed of nano- to-micrometer diameter fibers. The non-woven nature of the electrospun scaffold results in a tissue-engineering platform with a large surface area and highly interconnected pore spaces [9]. This architecture mimics the organization of the native extracellular matrix and can be tailored to selectively support a wide variety of cell types.

The elaborate and interconnected network of the native extracellular matrix exhibits varying degrees of anisotropy. The recapitulation of this structural feature may represent a critical design feature in the fabrication of tissue-engineered tendons, ligaments, blood vessels and other organs that may be subjected to uniaxial mechanical loads. This observation is especially important in light of growing evidence that fiber alignment and overall scaffold anisotropy play central roles in defining the material properties of electrospun materials [10–12]. Anisotropic properties can also be expected to represent a source of guidance cues that can be exploited to regulate cell phenotype, cell migration, and the distribution of cells within an engineered tissue [13, 14]. Our goal is to develop non-invasive techniques that can be used to objectively measure fiber alignment and overall scaffold anisotropy.

Morphological techniques and destructive materials testing strategies have been used to illustrate and detect anisotropy in electrospun materials. For example, we, and other authors, have used representative scanning electron micrographs to demonstrate fiber alignment in scaffolds prepared from various electrospun polymers [2, 6, 15, 16]. This approach lacks precision and is obviously highly subjective. Materials testing can be used to detect directional bias and evidence of scaffold anisotropy [6]. However, without an objective measurement of fiber alignment, it is difficult, at best, to determine how specific degrees of anisotropy might contribute to the biological, and mechanical, performance of a given scaffold.

Optical techniques, that are non-destructive, such as laser scattering, have been used to evaluate fiber orientation in valve leaflets [17, 18]. This elegant technique can resolve information to the level of individual fibers; however, it requires intensive data analysis to extract the descriptive parameters necessary to map the large-scale structural properties of a fibrous construct. Derivatives of Fourier transforms have long been used to measure the geometric composition of data images [19, 20] and, to a lesser extent, have been applied to the analysis of biological systems. For example, these algorithms have been used to evaluate the impact of specific genetic manipulations on cardiac cytoarchitecture and myofibrillar organization [21]. In limited applications of this technique, electrospun scaffolds have been processed for scanning electron microscopy and subjected to a custom image analysis strategy designed to track and map fiber distribution [11]. Unfortunately, this approach limits data acquisition to surface features and the sample is lost to the analysis. In this review, we describe how a two-dimensional fast Fourier transform (2D FFT), readily available in a number of programs designed for image analysis, can be coupled with a variety of optical imaging modalities to rapidly measure scaffold anisotropy [10, 12].

MATERIALS AND METHODS

Electrospinning

Reagents were purchased from Sigma–Aldrich unless noted. Gelatin was suspended at various concentrations (100, 120, 150 or 180 mg/ml) and agitated in 2,2,2-trifluoroethanol (TFE) for 24 h [8, 10, 12]. Electrospinning suspensions were loaded into a 20 ml Becton Dickinson syringe capped with an 18 gauge blunt-tipped needle. The air gap distance between the source suspension and the grounded target mandrel was set to 20 cm. A Harvard perfusion pump was used to meter the delivery of the electrospinning suspensions to the electric field; an accelerating voltage of 25 kV was used for all samples. The positive output lead of a high voltage power supply (Spellman CZE1000R; Spellman High Voltage Electronics) was attached by an alligator clip to the blunt tipped needle. A stainless steel rectangular (70 mm × 10 mm × 5 mm) mandrel designed to rotate from 0 to 6000 rpm was used as the grounded target. A digital stroboscope (Shimpo Instruments DT3-11A) was used to continuously monitor the target RPM. Samples were stored in a desiccation chamber to limit hydration prior to analysis.

Scanning electron microscopy

Dry, unfixed electrospun samples were sputter-coated for conventional scanning electron microscopy (SEM, Zeiss EVO 50 XVP). SEM images are amenable to 2D FFT analysis; however, data are restricted to the superficial surfaces of the specimen. Refer to the text for a discussion of the technical issues encountered when using this imaging modality.

Light microscopy

Scaffolds were imaged with a Nikon TE300 microscope equipped with a Nikon DXM 1200 digital camera. Images were captured using a 20 × 0.40 n.a. brightfield objective and stored as uncompressed .TIF files with an image dimension of 3840 × 3072 pixels. The theoretical lateral resolution of the 20× lens used in this study is 0.838 μm; the average fiber diameter of the scaffolds presented in this study is greater than 0.8 μm.

For routine 2D FFT analysis of scaffold structure, objective resolving power is matched to average fiber diameter. If an objective with inadequate resolving power is used to capture data sets, individual fibers are not detected and the resulting image is composed largely of optical noise. In general, this type of optical image/data set is unsuitable for analysis. We note, however, that under some circumstances the birefringence generated by sub-resolution fibers can be used to generate alignment data (see Ref. [10] for an example). In this type of data set, image alignment values should be interpreted with caution and an external measure of alignment (for example materials testing) should be used to calibrate the reported 2D FFT values derived under these conditions. While the selected

objective should have sufficient resolving power to image individual fibers, we attempt to keep objective magnification to a minimum. As objective magnification is increased, the total amount of surface area that is available for image capture is reduced. We believe that measurements of scaffold anisotropy should be averaged over as large as an area as possible. Local variations in fiber alignment can bias the 2D FFT process. If necessary, alignment data can be captured from several sites in a scaffold and averaged to circumvent the limitations inherent when a small sample surface area must be used to generate an alignment value.

Model scaffold

Thin spaghetti (Mueller's, American Pasta Company) was used to fabricate "model" scaffolds and to demonstrate how the 2D FFT generates and encodes alignment data. This material is easy to manipulate and allows for a variety of parameters to be explored. The thin spaghetti was arrayed in an uncooked or cooked (al dente, 5 min) state onto a flatbed scanner. Images were captured at 2048 × 2048 pixels and stored as grayscale .TIF files.

Confocal laser scanning microscopy

A Leica TCS-SP2 AOBS confocal laser scanning microscope was used to capture images of electrospun scaffolds. The pinhole was optimized for all images to 1 Airy disk unit. The 514 nm laser line was used to illuminate the samples; images were captured at a scan resolution of 2048 × 2048 pixels in reflectance mode. Representative cross-sections in the confocal data sets were calculated and projected along the x- and y-orientations (i.e., x–z and y–z digital slices). Electrospun samples were imaged with a 20× (0.70 n.a.) dry objective lens. Total surface area measured was 750 × 750 μm. The Voxel dimensions for this image are 0.36 × 0.36 × 0.36 μm. Confocal three-dimensional data sets were compiled as an average intensity data image and processed by 2D FFT. Alignment analysis of confocal images is sensitive to the method used to compile a 2D projection of a three-dimensional data set. We prefer to use an average projection in this type of analysis. While maximal projections can be used, average projections should only be compared to average projections and maximal projections should only be compared to maximal projections in 2D FFT analysis.

Demonstration of scaffold response to strain

Scaffold response to uniaxial stretch was characterized using a custom-fabricated stretching device. The instrument was modeled after a device used in previously published studies to examine cellular response to static loads [13]. The device resembles the original design but was re-manufactured from aluminum to lend additional stiffness to the stretching platform. Stretch was applied by a set of calibrated thumbscrews that displace a set of specimen clamps a known distance.

The stretching device was threaded to the stage of a Nikon TE 300 microscope. Dog-bone-shaped samples (2.67 mm wide with a gauge length of 7.49 mm) of electrospun scaffolds were mounted in the testing apparatus and held directly over the objective light path. A given area was repeatedly photographed as calibrated degrees of stretch (5, 15 and 25%) were placed across the sample.

2D Fast Fourier Transform

A more detailed description of the 2D FFT approach for measuring scaffold anisotropy is presented in the results section of this manuscript. All images were stored and analyzed as uncompressed .TIF files to preserve image integrity; the image compression used in .JPG format will degrade image integrity and should not be used for archival storage. Grayscale 8-bit images were cropped to 2048 × 2048 pixels for analysis. ImageJ software (NIH, http://rsb.info.nih.gov/ij) supported by an oval profile plug-in (authored by William O'Connnell) was used to conduct 2D FFT analysis. All alignment data was normalized to a baseline value of 0 and plotted in arbitrary units ranging from 0 to approximately 0.15.

Angle information concerning the principle direction of fiber alignment must be calibrated to the specific version of the NIH ImageJ software and oval profile plug-in used for analysis. Convention places the 0° position (Fig. 1B) at 3:00 o'clock on the unit circle and continues in a counterclockwise fashion with 90° at 12:00 o'clock, 180° at 9:00 o'clock and 270° at 6:00 o'clock. Some versions of ImageJ (1.36b) altered this convention and 0° was placed at 9:00 o'clock and continued in a clockwise fashion. Minor corrections were incorporated into our analysis to correct for this condition, but may not be necessary for all 2D FFT programs.

To produce the window mask (Fig. 3K), scaffold images were imported into and cropped using Adobe Photoshop (Adobe Systems). The window mask should be constructed with a gradation of grayscale pixels (darkest at the periphery, lightest at the inner ring). Scaffold images were cut with the elliptical marquee tool into circular samples and the edges were set to feather by 20–25 pixels. These circular data images were then placed onto a grayscale window and flattened prior to 2D FFT analysis.

Materials testing

Following 2D FFT analysis, samples were subjected to materials testing using a Bionix 200 Mechanical Testing Systems instrument equipped with a 50 N load cell (MTS Systems). Samples were cut into a series of dog-bone-shaped samples (2.67 mm wide with a gauge length of 7.49 mm). Specimen thickness was determined with a Mitutoyo IP54 digital micrometer. Scaffolds were tested to failure using an extension rate of 10 mm/min to evaluate the stress, strain and modulus of elasticity [10, 12].

RESULTS

Overview

The 2D FFT function converts spatial information in an optical data image into a mathematically defined frequency domain. This frequency domain maps the rate at which pixel intensities change in the spatial domain. Figure 1 provides an overview of how the output of this process is used to measure fiber alignment. A subjective evaluation of the depicted brightfield images (Fig. 1A, D and G) indicates that each scaffold is composed of fibers with varying degrees of alignment.

For analysis, grayscale brightfield microscopic images were captured and converted to an integer power of 2 pixel dimensions (256×256, 512×512, 1024×1024, etc.). If images have been captured in color they must be converted to grayscale for

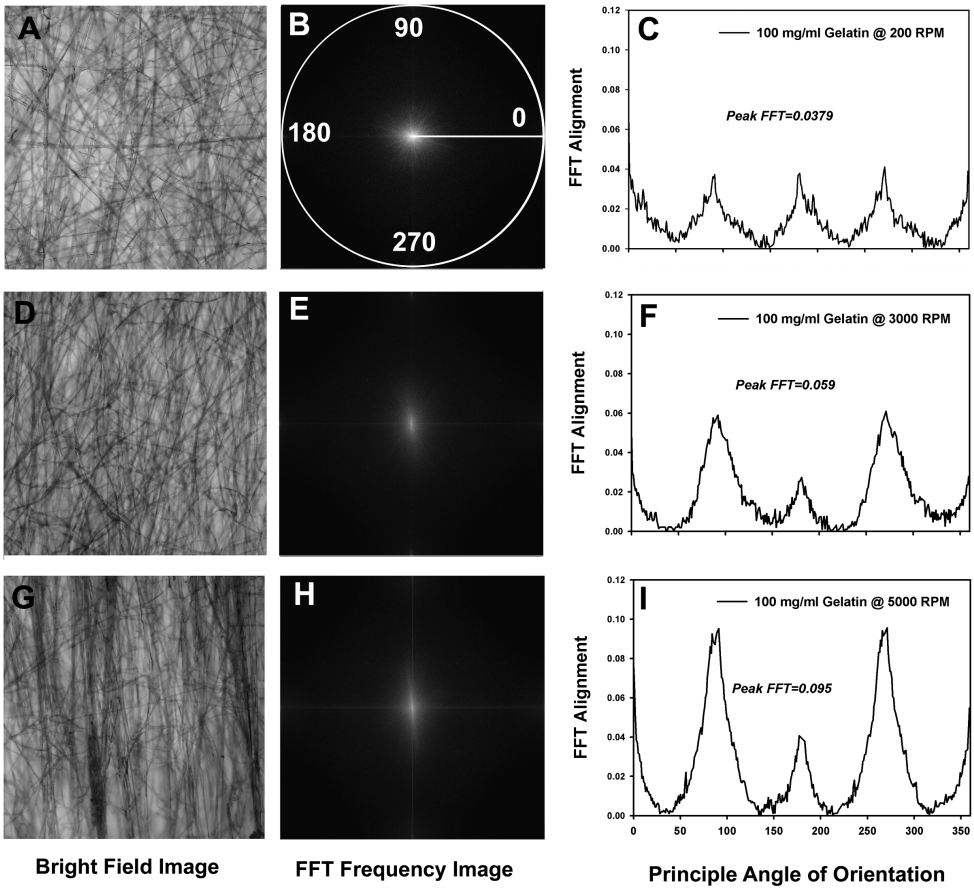

Figure 1. 2D FFT analysis of scaffold anisotropy. Bright field images of representative electrospun scaffolds (A, D, G). ImageJ frequency plots (B, E, H) and 2D FFT alignment plots (C, F, I) for the corresponding bright field images. Note that peak shape and height in the 2D FFT alignment plot report the relative degree of alignment present while the peak position reports the principle axis of orientation for the fiber field.

2D FFT analysis. Care should be taken at the time of image capture to optimize sample illumination; uneven illumination can complicate and introduce error into the alignment analysis (see discussion in the normalization section of this paper).

Processing a brightfield data image by 2D FFT produces a frequency plot, or power spectrum. This plot is composed of grayscale pixels that are distributed into a pattern that can be used to measure the degree of fiber alignment present in an original data image (Fig. 1B, E, H). The frequency plot produced by NIH ImageJ software places low frequency pixels at the origin, or center, of the frequency plot (note: selected iterations of the FFT function invert this convention and place low frequency pixels at the image periphery). Low-frequency signals correspond to domains within the original microscopy image that contain pixels of similar values, adjacent pixels do not vary to a great extent in intensity. The bulk of this information originates with the background and the overall shape of the image. High-frequency pixels are placed away from the origin and toward the periphery of the frequency plot. This information corresponds to spatial domains that exhibit abrupt changes in pixel intensity. Edges, details and noise in the data image all contribute to the generation of high-frequency pixels.

When an image of random fibers is processed by 2D FFT, the resulting frequency plot contains a cluster of white pixels that are concentrated in a symmetrical, circular pattern around the origin (Fig. 1B). At this point in the process we rotate the frequency plot 90° (the direction is irrelevant) to correct for the inherent rotation of the data that is induced by 2D FFT analysis. A circular projection is placed on the frequency plot (using the ImageJ circular marquee tool). Using the ImageJ oval profile plug-in the pixel intensities are then summed along the radius for each angle of the circular projection (0–360°; see Fig. 1B for an example of a circular projection and a single radius). The summed pixel intensities for each radius are then plotted against the corresponding angle of acquisition (position of the radial projection on the circular projection) to produce a 2D FFT alignment plot (Fig. 1C). Typically, the data from this analysis is reported for 0 to 180°; the frequency plot is symmetric so a complete summation from 0 to 360° is not technically necessary. The images and plots in Fig. 1 demonstrate this symmetrical property of the 2D FFT process.

The 2D FFT alignment plot of a random matrix will exhibit 4 peaks that occur every 90°. Peaks of nearly uniform height are a hallmark of a scaffold composed of random elements. These peaks reflect low-frequency spatial information and edge artifacts. An analysis of the scaffold composed of random fibers illustrated in Fig. 1A generates a peak 2D FFT alignment value of 0.038 units. For a gelatin-based scaffold with this alignment value, there will be no evidence of directional bias during destructive materials testing; average stress and strain at failure will be similar regardless of the direction that a test load is placed across this type of sample [12]. When brightfield data images are processed by 2D FFT, evidence of directional bias in materials testing develops at an alignment value of approximately 0.05 units [10, 12].

If a data image containing aligned fibers is processed by 2D FFT, the resulting frequency plot contains pixels that are concentrated along a specific axis (Fig. 1D, E, G and H). An examination of this type of frequency plot prior to rotation reveals that the high-frequency pixels that report alignment will be preferentially arrayed 90° with respect to the principle angle of fiber orientation. By rotating the frequency plot 90° prior to the radial summation step, the principle angle of fiber orientation can be directly obtained from the alignment plot (e.g., Fig. 1F and I). During radial summation the preferentially arrayed pixels act to increase the summed pixel intensity value along a defined axis, producing a prominent peak in the 2D FFT alignment plot. The 2D FFT alignment plots generated from sample scaffolds containing aligned elements exhibit asymmetrical peaks, two larger peaks at 90 and 270° and two smaller peaks at 0 and 360° (Fig. 1F and I). The degree of alignment present in the original data image is reflected by the height and overall shape of the most prominent peaks present in the alignment plot. A high and narrow peak indicates a more uniform degree of fiber alignment, a broad peak, or a shoulder on the peak indicates that more than one axis of alignment may be present. The principal axis of fiber alignment is determined by the position of the alignment peaks, in the illustrated examples (Fig. 1F and I) the principle axis of alignment is in the vertical direction in the processed image.

Specific degrees of alignment can be correlated with the onset of distinctive material properties. These material properties develop largely independent of fiber diameter [12]. When processing a brightfield data image by 2D FFT we observe the onset of anisotropic properties in an electrospun scaffold of gelatin at a threshold alignment value of 0.05 units. For example, the stress at failure for a random scaffold (Fig. 1C) of electrospun gelatin (2D FFT alignment value <0.05 units) is approximately 0.5 MPa in all directions. Once alignment values of 0.05 units are detected this type of scaffold, stress at failure will increase incrementally as a function of approximately 0.01 2D FFT alignment units. In a moderately aligned scaffold (similar to Fig. 1D) with a 2D FFT alignment value of 0.05–0.06 units the stress at failure increases to 0.75 MPa in parallel with the principle axis of fiber orientation. At 2D FFT alignment values of 0.06–0.07 units, stress at failure is approximately 1.0 MPa and, at alignment values of 0.07 to 0.08 units, stress at failure increases to 1.5 MPa when the test load is applied in parallel with the principle axis of fiber orientation [12].

Normalization and edge noise

Normalization is necessary to account for differences in sample thickness, camera performance, operator preference for contrast/brightness, and other variables that impact sample illumination at the time of image capture. The end result of this process is to place data generated from a variety of images onto a common scale. Figure 2 illustrates and provides a validation of the normalization process. The raw 2D FFT alignment plots generated from a series of 5 brightfield microscopic images of a single sample are depicted in Fig. 2A. Each image contained the same field of

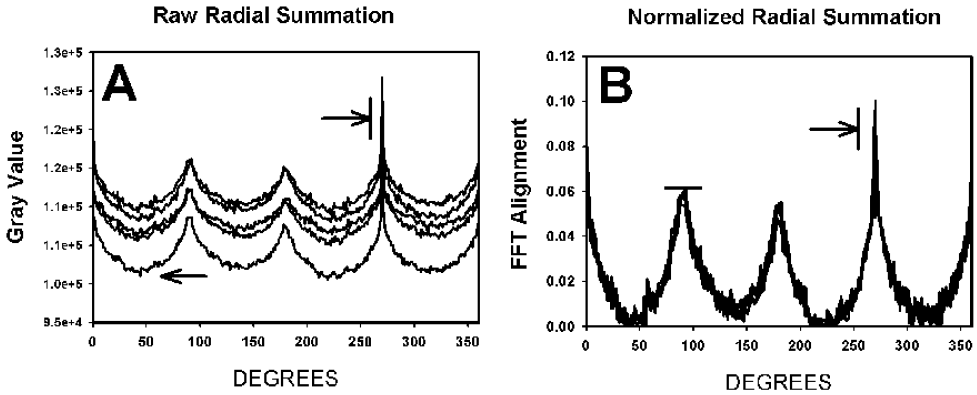

C

A.	B.	C.	D.	E.		F.
Angle of Acquistion (Degree)	Summed Pixel Intensity	Normalization Value	Intensity/ Normalization (B/C)	2D FFT Alignment Value (B/C)-1		Sorted Pixel Intensity
0	112323.00	106666.26	1.053032159	0.053032159		105972.28
1	111537.34	106666.26	1.045666531	0.045666531		106361.15
2	111423.70	106666.26	1.044601143	0.044601143		106405.56
3	110492.16	106666.26	1.035867931	0.035867931		106414.61
4	110523.30	106666.26	1.036159879	0.036159879		106424.50
5	110204.74	106666.26	1.033173415	0.033173415		106502.50
6	110556.63	106666.26	1.03647233	0.03647233		106545.52
7	109768.86	106666.26	1.029086996	0.029086996		106550.01
8	110421.84	106666.26	1.035208679	0.035208679		106550.30
9	110086.47	106666.26	1.032064601	0.032064601		106613.32
10	109250.09	106666.26	1.024223555	0.024223555		106646.27
11	109227.61	106666.26	1.024012758	0.024012758		106651.67
12	108745.84	106666.26	1.019496118	0.019496118		106666.26
13	108941.67	106666.26	1.021332088	0.021332088		106670.34

Figure 2. Normalization. Panel A illustrates the alignment plots for a series of 5 photographs taken of the same fiber field at varying light intensities. As the average light intensity used to capture an image increases the uncorrected alignment plot is displaced upward on the y-axis. The arrow in A denotes a spurious peak associated with edge noise. The arrow at the base of the alignment plot (A) denotes the lower regions of the trace that should be brought in contact with the x-axis during normalization. Panel B illustrates the data depicted in panel A after normalization. The arrow in B again denotes edge noise; note normalization does not remove this spurious noise. It is visually removed from the data set. Actual alignment value is denoted by the line at the top of the peak present at approximately 90°. Panel C illustrates the normalization process. See text for complete description.

fibers but was captured at varying light intensities. The shape of the data trace for each alignment plot is similar in nature; however, the summed pixel intensity values generated from the radial summation step varies considerably for each image. Images taken with greater light intensity at image capture have, on average, higher

pixel values and are displaced upwards on the y-axis. Figure 2B illustrates this same set of data after normalization; the 2D FFT alignment plots for the images overlap and report a common 2D FFT alignment value (approximately 0.06 units at 90°). These results indicate that the 2D FFT approach can be applied to images captured over a wide range of conditions. However, note that, as light intensity increases, the relative amount of optical noise present in a brightfield microscopic image also will increase. Detector noise functions in an inverse fashion. As light intensity is decreased and detector gain is increased to generate an image, electronic noise begins to be incorporated into the data set. Noise from either source (optical and/or electronic) can introduce artifacts into a data image and adversely impact the 2D FFT process.

Under ideal conditions, normalization will place each of the four baseline values of the 2D FFT alignment plot in contact with the x-axis (compare Fig. 2A before normalization with Fig. 2B after normalization). If the normalization factor is too large, the calculated alignment value will be underreported (because the baseline values of the alignment plot are displaced below the x-axis). Conversely, if the factor is not large enough, the alignment value will be exaggerated (because the plot is displaced upward on the y-axis like the plots illustrated in Fig. 2A).

Figure 2C provides an example of normalization. Columns A and B represent the radial summation data as exported from ImageJ into an Excel spreadsheet (for brevity only the first 13° of data are displayed, the complete set will contain 360° of data). A candidate normalization factor can often be selected by copying the original radial summation data set (Fig. 2C, column B) into a new column and sorting this duplicate column in ascending order (Fig. 2C, column F). In the illustrated example, the pixel intensity value that resides in the 12th position of the sorted pixel intensity column was selected as the normalization factor (Fig. 2C column F: 106666.26). Once a candidate normalizing factor has been chosen, the pixel intensity value for each angle in the original radial summation data set (Fig. 2C, column B) is divided by this value (Fig. 2C, Column C). We prefer to rescale the alignment data by subtracting 1 from the output of this manipulation (Fig. 2C, column D − 1 = column E). To generate our version of the final alignment plot, the normalized 2D FFT alignment values (Fig. 2C, column E) are plotted against the angle of acquisition (Fig. 2C, column A).

Normalization is tolerant to a degree of error; small deviations around the "perfect value" will not overtly corrupt the alignment plot. Uneven sample illumination at the time of image capture will manifest itself at this point in the process. The baseline values of an alignment plot generated from an image captured under these conditions cannot be uniformly rectified with the x-axis; the data trace fails to parallel the x-axis. It may be necessary to re-capture the original data image under these circumstances, if this option is not available it may be possible to apply a rolling filter to the existing image to correct the defect (see ImageJ software, select: Process menu, Subtract background, for additional strategies and discussion see also Ref. [22]).

Edge effects can and will add spurious information to the peaks of an alignment plot. The contribution of this of type of noise to a 2D FFT image will be most pronounced in a data set containing aligned fibers that are arrayed at approximately 45° with respect to the border of the image. The 2D FFT function replicates the data image and assembles the duplicate images into a series of "tiles" that resemble a parquet floor. The intersection of fiber edges at the interface of the "tiles" in this parquet floor produces the bulk of edge noise. Edge noise is usually obvious and can be easily discarded by visual inspection of the plotted data. Figure 2B provides an example of a normalized 2D FFT alignment plot containing a corrected (edge noise removed) and uncorrected (edge noise not removed) peak. The corrected peak (seen at 90°) has a 2D FFT alignment value of approximately 0.065 units, whereas the uncorrected peak (seen at 270°) has a 2D FFT alignment value of approximately 0.10 units. Edge noise is usually very distinctive and produces a sharp, prominent spike in the alignment plot. In Fig. 3D a discrete set of lines (that divide this image into 4 quadrants) is present in the frequency plot. When a radial summation is applied to a frequency plot containing this artifact, the resulting 2D FFT alignment plot will contain a large spike (as illustrated in Fig. 2B).

The overall 2D FFT alignment value for a scaffold is determined by visually inspecting and selecting the maximal value from the peak of the alignment plot. A highly aligned scaffold imaged by brightfield microscopy will produce a 2D FFT alignment value of approximately 0.12 units on our scale; for the same fiber field a confocal image will generally produce a slightly higher value (see Ref. [10] for examples).

2D FFT frequency plot

Model scaffolds were manipulated into varying patterns and imaged to demonstrate how scaffold structure modulates the output of the 2D FFT function and to illustrate how alignment information is encoded and reported by the frequency plot (Fig. 3).

First, consider a model scaffold composed of straight fibers that have been arrayed into a fan-shaped pattern (Fig. 3A). If the frequency plot is rotated 90° prior to inspection, the high-frequency pixels present in this plot will be arrayed into a pattern that mimics the fan-shaped array of fibers that were present in the original data image. These high-frequency pixels are generated by the fiber edges, the banded pattern that is evident reflects the spacing of the fibers (Fig. 3B). Information concerning fiber spacing is usually lost when a "real" scaffold is processed by the 2D FFT approach. The fibers of an electrospun scaffold are rarely uniformly spaced and they overlap, curve and pass in and out of the plane of focus. The generated 2D FFT alignment plot of the fan array is noisy and continually changing to report the different angles of orientation that occur across the fiber field. Since there is no specific orientation present, no favored polarity will be detected and the 2D FFT alignment value for this model scaffold will be small (Fig. 3M, arrayed fan plot).

The random model scaffold illustrated in Fig. 3C is composed of curving fibers and likely contains as many fiber edges as the fan-shaped model scaffold (Fig. 3A).

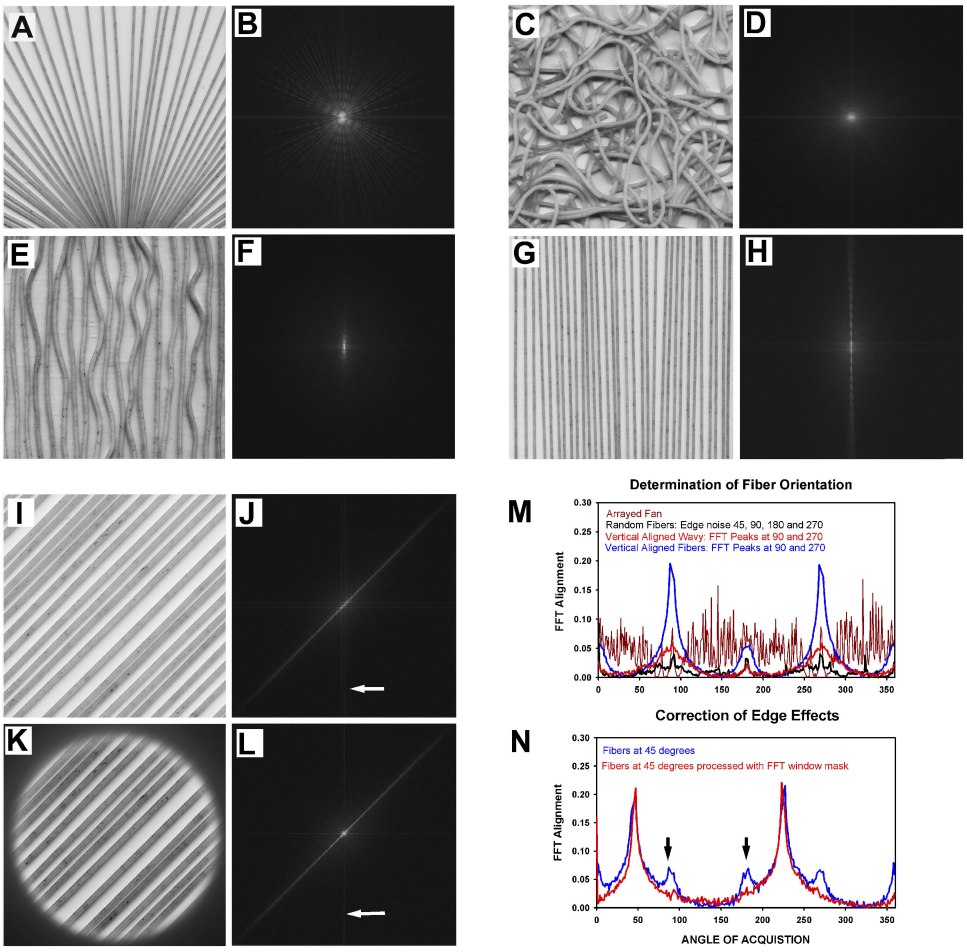

Figure 3. Frequency plots generated from model scaffolds. (A–H) Images of the model scaffolds and corresponding frequency plots, see text for discussion. Panels I–L demonstrate the attenuation of edge effects (arrows in J and L) in a data image through the use of a Window mask. (M) 2D FFT alignment plots generated from model scaffolds and illustrated frequency plots. (N) 2D FFT alignment plots before and after removing edge effects from the images depicted in panels I–L. Arrows denote edge noise artifacts. This figure is published in colour at http://www.ingenta.com

The pixel values that correspond to these edges must undergo constant fluctuations to map the curving trajectory of the fibers present in the spatial domain. The frequency plot of this scaffold contains a cluster of low frequency pixels near the origin with the high-frequency pixels dispersed in a symmetrical pattern about the origin (Fig. 3D). There is no evidence of a preferential orientation or distribution to these pixels, and the 2D FFT alignment plot generated from this data is a smooth trace containing 4 small, symmetrical peaks (Fig. 3M, random fiber plot).

A field of aligned, slightly undulating fibers (which more closely resembles the fibers of an aligned electrospun scaffold, Fig. 3E) produce high-frequency pixels

that are preferentially distributed along the vertical axis of the frequency plot (once the plot has been rotated 90°, Fig. 3F). The 2D FFT alignment plot of this scaffold (Fig. 3M, vertical aligned wavy plot) contains distinct peaks at 90 and 270° (2D FFT alignment value of 0.06 units) and much smaller peaks at 180 and 360° (2D FFT alignment value of 0.02 units). The larger peaks report the principle axis of alignment while the smaller peaks correspond to background information, noise and edge effects (Fig. 3M).

The effect of fiber alignment on the concentration of high-frequency pixels along a specific axis in the frequency plot is easily demonstrated using a field of fibers that are straight and arranged in parallel (Fig. 3G, H and M). In order to generate a spatial map of the vertical edges of these fibers, the pixels of the data image must undergo regular transitions along the horizontal axis in the original data image. The 2D FFT reports this condition as a preferential distribution of high-frequency information and the resulting frequency plot contains pixels that are distributed along a narrowly defined axis. When summed, these high-frequency pixels produce a characteristic trace on the 2D FFT alignment plot. The alignment peaks are narrow and sharply delineated, indicating nearly uniform fiber alignment (Fig. 3M, vertically aligned fiber plot). If a fraction of the fiber population is oriented off the principal axis of orientation the 2D FFT process will produce a broader alignment peak or a peak with a shoulder.

As noted in the previous sections, edge effects and background noise (and detector noise) can "spill over" and obscure data in the 2D FFT frequency and alignment plots. This noise effect is quite pronounced in a model scaffold containing aligned fibers that are arrayed approximately 45° with respect to the edges of the image (Fig. 3I, arrow in J indicates noise). Noise of this nature can be greatly diminished by placing a grayscale window mask over the fiber field prior to analysis (Fig. 3K, arrow in L indicates the reduced noise). The unmasked image produces a 2D FFT alignment plot with artifacts in the guise of small peaks on either side of the alignment peaks (Fig. 3N, arrows). Processing the image with a window mask removes this spurious information without altering the height of the alignment peaks (i.e., 2D FFT alignment value, Fig. 3N). Although this type of mask can be useful in many applications, it reduces the total surface area available for analysis. In the illustrated example the spurious peaks are small with respect to the alignment peak; in an electrospun scaffold the artifacts produced by edge noise and the data encoding alignment will produce peaks of similar magnitude.

High-resolution microscopy can detect and report considerable variation in pixel intensity across a single fiber. This type of spatial information can add high frequency noise to the 2D FFT frequency plot, partially masking alignment data. SEM images of electrospun scaffolds, where information and variations in contrast are resolved across the diameter of individual fibers, are particularly susceptible to producing this form of interference. One solution that can be applied to reducing this type of interference is to use the Back Scatter mode to capture the images. This imaging mode produces less contrast across the individual fibers than

conventional imaging modes. High-resolution pixel noise also can be reduced by passing a Gaussian filter across the original data image prior to 2D FFT analysis. This treatment reduces pixel variation and smoothes the data set. Conventional smoothing filters should be avoided; these filters can artificially induce polarity into a data set. Reducing pixel density at the time of image capture or in a digital image prior to 2D FFT processing also can be used to reduce high frequency noise. In practice, images should be captured at the same resolution under similar conditions. Threshold filters that compress and re-scale data to produce images composed exclusively of black and white pixels have utility in the processing of SEM images. Any use of a masking filter, Gaussian filter, rolling ball filter, threshold filter, or manipulation of pixel density should be uniformly applied to each image in a data set that is to be compared.

Dynamic applications

The 2D FFT approach can also be used to measure other aspects of scaffold structure and performance. For example, we use 2D FFT to examine how mechanical loads impact fiber orientation in tissue-engineering scaffolds. Figure 4 illustrates a series of experiments demonstrating this technique. In this experiment we sequentially photographed a dry scaffold as we placed a calibrated strain across the sample. The resulting images were then analyzed using the 2D FFT approach. The 2D FFT analysis of random scaffolds indicates that fiber alignment remains constant (Fig. 4A), failure occurred at a site distal to the actual domain imaged.

When a dry scaffold composed of aligned fibers was stretched in parallel with the principal axis of anisotropy there was a nominal increase in the 2D FFT alignment value prior to failure (from 0.08 to 0.11 units at 5.0% stretch, Fig. 4B). Applying stretch in a tangential fashion to an aligned matrix induced modest changes in the principal angle of fiber orientation prior to scaffold failure (not shown). We conclude from these experiments that strains are not uniformly distributed throughout a dry scaffold, failure (fracture) occurs at a specific site in the construct. We believe that fibers in a hydrated state would undergo far more re-alignment in response to strain than in a dry specimen.

Future directions

Electrospun fibers appear to deposit as discrete layers onto the target mandrel. To further modulate the material and biological properties of an electrospun scaffold, we are interested in developing strategies to induce more fiber entanglement in the z-direction and using 2D FFT to evaluate the trajectory of these fibers. For example, consider the confocal image presented in Fig. 4C that is composed of fibers that are predominately arrayed along the vertical orientation of the image. Conventional 2D FFT analysis of this confocal image generates an alignment value of 0.17 units (moderately aligned for a scaffold captured by confocal imaging). It is possible to verify fiber orientation in this scaffold by surveying the confocal three-dimensional

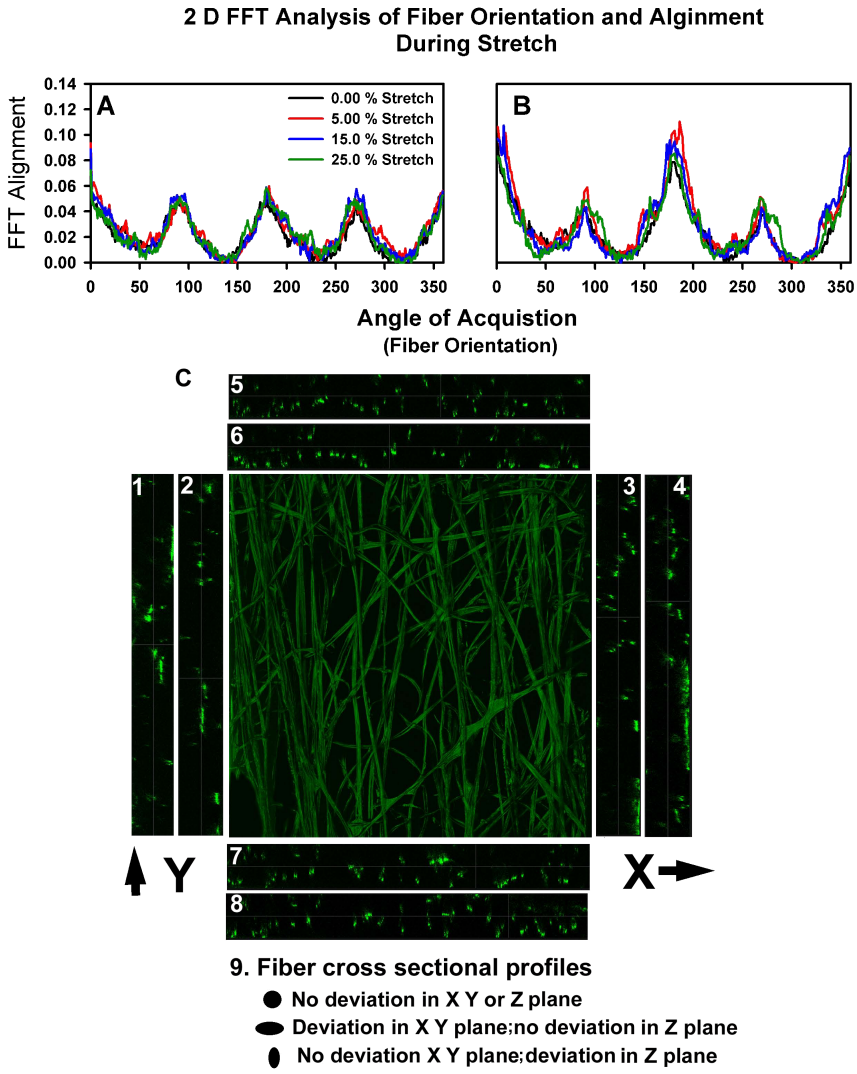

Figure 4. Use of the 2D FFT in dynamic applications and laser confocal microscopy. (A) 2D FFT alignment plots of a random scaffold at 0, 5, 15 and 25% stretch. Fibers of a dry, random scaffold do not undergo re-distribution in response to applied strain. (B) 2D FFT alignment plot of a partially aligned scaffold at 0, 5, 15 and 25% stretch. A nominal change in fiber alignment was detected in this sample at 5% stretch. (C) Confocal data set compiled as an average projection. Subsections 1–4: Cross-sections imaged in the y-orientation (i.e., y–z planes). Subsections 5–8: Cross-sections imaged in the x-orientation (i.e., x–z planes). Subsection 9 illustrates theoretical cross-sectional profiles observed when fibers traverse an optical plane (note: simultaneous deviations in x, y and z planes are not illustrated). We note that very precise fiber cross-sectional diameters can be generated by scanning confocal microscopy when this modality is coupled with de-convolution analysis (this manipulation will also reduce high-frequency noise) of the data set. For 3D data sets that contain isometric voxels (for example, $0.2 \times 0.2 \times 0.2$ µm) it is theoretically possible to conduct 2D FFT image analysis on each of the cross-sectional profiles (x, y and z projections) to calculate alignment and fiber trajectory data. This figure is published in colour at http://www.ingenta.com

data set in cross-section. Representative cross-sections of the illustrated example in the x- and y-axis reveals a higher frequency of elongated fiber profiles in the y-axis (aligned fibers cut longitudinally; Fig. 4C, panels 1–4) than in the x-axis. This structure occurs because fibers are arrayed in parallel with the y-axis. In contrast, fiber profiles in the x-axis are predominately round or oval in shape (aligned fibers cut in cross-section; Fig. 4C, panels 5–8). At present we are adapting our optical methods to measure the shape of the cross-sectional profiles of fiber populations in large, three-dimensional confocal data sets. This information can be used to map and measure the trajectory of individual fibers in the x-, y- and z-directions (Fig. 4C, panel 9). The cross-sectional profile of individual fibers also can theoretically be used to extrapolate fiber trajectory information using the 2D FFT function.

DISCUSSION

Electrospun materials can be uniquely tailored to specific tissue-engineering applications to mimic the physical, biological and material properties of the native extracellular matrix. For example, fiber diameter and pore dimension of a given polymer scaffold can be largely controlled by regulating the concentration of polymer (viscosity and degree of chain entanglements) present in the starting solution [6, 10] and/or the electrospinning air gap, accelerating voltage [15, 23, 24] and/or target properties [10]. Biological activity can be manipulated by controlling fiber identity and the overall composition of the electrospun tissue-engineering scaffold [8]. Growth factors and other pharmaceuticals can be selectively added to the scaffolds during and/or after the electrospinning process [25]. Material properties can be modulated by altering scaffold structure, composition, and through post-electrospinning processing events that increase fiber cross-linking [26].

The frequency plot of the 2D FFT function has been used to select, identify and measure the geometric composition of images in a broad spectrum of applications. Quantitative information concerning the orientation of objects in a data image also is encoded by this plot. By processing a digital image of an electrospun scaffold with the 2D FFT function it is possible to extract this information and use this data to assign a numerical value to the degree of fiber alignment present in the original sample [12].

The 2D FFT approach is a relatively simple technique to put into practice; however, there are clear limitations. For example, imaging modality and sample thickness must be considered prior to analysis. In brightfield microscopy samples must be thin enough to allow light to pass through the specimen. This imaging modality is most suited for samples composed of fibers arrayed in a homogenous fashion. Structures that exhibit discrete fiber layers that are engineered to display differing degrees of alignment in each layer are generally not suited for analysis by brightfield microscopy. This limitation exists because fibers out of the plane of focus can participate in generating data that is used by the 2D FFT function.

Constructs composed of complex multiple layers are better imaged by laser scanning confocal microscopy, an imaging technique that can be used to capture data from specific optical planes. For many proteins and selected synthetic polymers, images can be captured using an auto-fluorescence signal. We also have successfully used reflectance mode to capture images of scaffolds composed of biological [10] and synthetic materials [14]. This approach can be used to capture information for 30–40 μm of depth in the z-direction. For more extensive penetration, markers may be incorporated into scaffolds at the time of electro-processing. If appropriate, standard immunohistochemical methods can be used to stain and image scaffolds composed of native proteins. For extremely dense or thick (i.e., in the z-direction) electrospun constructs, the use of a two-photon confocal imaging system may be necessary. Note, as sample thickness increases, there will be increased photon scatter. Under these conditions deconvulsion analysis may be necessary to accurately construct the data set. Three-dimensional confocal data files, in general, are biased in the z-direction. In cross-sectional analysis, this bias will take a round profile and elongate it into an oval profile (for an excellent discussion of image restoration and deconvolution, see Ref. [27]). By analogy, for a model matrix composed of round spaghetti, z-direction bias would make this pasta appear flattened and elongated like linguini when viewed in cross-section. Deconvolution corrects this bias by reshaping the point spread function, a manipulation that takes on added importance when fiber alignment in multiple dimensions is to be calculated.

While we prefer to use confocal microscopy to characterize different fiber layers, it also is possible to generate similar information by sequentially sampling a specimen during the electrospinning process. In order to conduct this type of analysis the electrospinning process must be stopped to isolate a sample of each fiber layer. The individual samples can then be imaged and processed by 2D FFT. We do not recommend this strategy on a routine basis, unless necessary. Fiber layers may delaminate as a result of drying incurred during the sampling intervals, a condition that may adversely impact sample integrity and structure.

Finally, in the analysis of fiber alignment it is critical to consider precisely what scaffold anisotropy represents to each individual application. Certainly the 2D FFT approach can be used to verify the reproducibility of the electrospinning conditions and the structure of a scaffold. However, for most applications, some external measure of anisotropy or scaffold performance is usually necessary to calibrate the 2D FFT alignment value. For example, our principle objective has been to identify how fiber diameter and varying degrees of fiber alignment interact to modulate the material properties of an electrospun material [6, 10, 12]. The stress and strain properties of an idealized scaffold composed of random elements should be identical regardless of the testing angle. These material properties can be expected to develop directional bias and vary as increasing degrees of anisotropy are introduced into the matrix. We have used these characteristic properties to calibrate our 2D FFT alignment values. In our laboratories, an archival image of each scaffold is captured

and processed for 2D FFT analysis. The scaffold is then subjected to materials testing in the parallel and perpendicular orientations and analyzed using stress at failure [12]. In conventional materials testing this material property appears to track most closely with incremental changes in fiber alignment.

Applications in which the central objective is to promote the expression of a specific cell phenotype or provide a guidance cue may require a different external measure of performance. For example, we have examined how scaffold anisotropy can be used to promote neurite outgrowth in specific directions. This body of work suggests that electrospun scaffolds do not have to be composed of uniformly aligned arrays of fibers to direct the growth of neurons along a predefined axis [14]. Some yet to be defined threshold of alignment is necessary to achieve this objective, a result that has direct implications in the fabrication of nerve guides and other tissue engineered products designed to direct cell phenotype.

The 2D FFT approach has several advantages. Notably, software is readily available, easy to implement and very little specialized equipment is needed to generate objective measurements of alignment. A variety of different imaging modalities, including brightfield, laser scanning confocal and scanning electron microscopy, can be used to capture data for analysis. The technique is adaptable and we demonstrated that it can be used quantify dynamic changes in fiber alignment in response to mechanical loads. By coupling the 2D FFT approach with laser scanning confocal microscopy it is possible to generate alignment data in three dimensions and/or within specific optical planes. Notably, the non-destructive nature of the 2D FFT approach makes it possible to measure fiber alignment in a specific sample and subsequently use that scaffold in a tissue-engineering application.

Acknowledgements

This work supported in part by NIH R01EB003087 (D. G. S.) and NIH 5R21EB003407 (G. L. B.). Scanning electron microscopy and laser scanning confocal microscopy conducted in the VCU Department of Neurobiology & Anatomy Microscopy Facility, supported with funding from NIH-NCRR shared instrumentation grant (1S10RR022495) and, in part, NIH-NINDS Center core grant (5P30NS047463). D. G. S. and G. L. B. have US and International Patents Issued and Pending concerning the use of the electrospinning process.

REFERENCES

1. D. G. Simpson and G. L. Bowlin, *Expert Rev. Med. Devices* **3**, 9 (2006).
2. J. A. Matthews, G. E. Wnek, D. G. Simpson and G. L. Bowlin, *Biomacromolecules* **3**, 232 (2002).
3. G. E. Wnek, M. E. Carr, D. G. Simpson and G. L. Bowlin, *Nano Lett.* **2**, 213 (2003).
4. E. D. Boland, J. A. Matthews, K. J. Pawlowski, D. G. Simpson, G. E. Wnek and G. L. Bowlin, *Front. Biosci.* **1**, 1422 (2004).

5. E. D. Boland, G. E. Wnek, D. G. Simpson, K. J. Pawlowski and G. L. Bowlin, *J. Macromol. Sci*. **38**, 1231 (2001).
6. E. D. Boland, B. D. Coleman, C. P. Barnes, D. G. Simpson, G. E. Wnek and G. L. Bowlin, *Acta Biomater*. **1**, 115 (2005).
7. S. A. Sell, M. J. McClure, C. P. Barnes, D. C. Knapp, D. G. Simpson, B. H. Walpoth and G. L. Bowlin, *Biomed. Mater*. **1**, 72 (2006).
8. T. A. Telemeco, C. E. Ayres, G. L. Bowlin, G. E. Wnek, E. D. Boland, N. Cohen, C. M. Baumgarten, J. A. Matthews and D. G. Simpson, *Acta Biomater*. **1**, 377 (2005).
9. A. Frenot and I. S. Chronakis, *Curr. Opin. Colloid Interface Sci.* **8**, 64 (2003).
10. C. E. Ayres, G. L. Bowlin, S. C. Henderson, L. Taylor, J. Schultz, J. K. Alexander, T. A. Telemeco and D. G. Simpson, *Biomaterials* **27**, 5524 (2006).
11. T. Courtney, M. S. Sacks, J. Stankus, J. Guan and W. R. Wagner, *Biomaterials* **27**, 3631 (2006).
12. C. E. Ayres, G. L. Bowlin, R. Pizinger, L. Taylor, C. A. Keen and D. G. Simpson, *Acta Biomater.* **3**, 691 (2007).
13. D. G. Simpson, M. Majeski, T. K. Borg and L. Terracio, *Circ. Res.* **85**, e59 (1999).
14. W. Chow, D. G. Simpson, J. W. Bigbee and R. J. Collelo, *Neuron Glia Biol*., in press (2007).
15. R. Kessick, J. Fenn and G. Tepper, *Polymer* **45**, 2981 (2004).
16. F. Yang, R. Murugan, S. Wang and S. Ramakrishna, *Biomaterials* **26**, 2603 (2005).
17. M. S. Sacks, D. B. Smith and E. D. Hiester, *Ann. Biomed. Eng.* **25**, 678 (1997).
18. M. S. Sacks and F. J. Schoen, *J. Biomed. Mater. Res.* **62**, 359 (2002).
19. M. K. Moell and M. Fujita, *IAWA J.* **25**, 311 (2004).
20. P. P. M. van Zuijen, H. J. C. de Vries, E. N. Lamme, J. E. Coppens, J. van Marle, R. W. Kreis and E. Middelkoop, *J. Pathol.* **198**, 284 (2002).
21. W. J. Karlon, J. W. Covell, A. D. McCulloch, J. J. Hunter and J. H. Omens, *Anat. Rec.* **252**, 612 (1998).
22. F. J. Leong, M. Brady and J. Q. McGee, *Clin. Pathol.* **56**, 619 (2003).
23. J. Doshi and D. H. Reneker, *J. Electrostat.* **35**, 151 (1995).
24. J. M. Deitzel, J. Kleinmeyer, D. Harris and N. C. B. Tan, *Polymer* **42**, 261 (2001).
25. E. Kenawy, K. Mansfield, G. L. Bowlin, D. G. Simpson and G. E. Wnek, *J. Control. Rel.* **81**, 5 (2002).
26. C. P. Barnes, C. W. Pemble IV, D. D. Brand, D. G. Simpson and G. L. Bowlin, *Tissue Eng.* **13**, 1593 (2007).
27. L. Landmann and M. Marbet, *Micro Res. Tech*. **64**, 103 (2004).